

Electronic Supplementary Material

Shaped Pt–Ni nanocrystals with an ultrathin Pt-enriched shell derived from one-pot hydrothermal synthesis as active electrocatalysts for oxygen reduction

Jun Gu^{1,§}, Guangxu Lan^{1,§}, Yingying Jiang^{2,§}, Yanshuang Xu¹, Wei Zhu¹, Chuanhong Jin², and Yawen Zhang¹ (✉)

¹Beijing National Laboratory for Molecular Science, State Key Laboratory of Rare Earth Materials Chemistry and Applications, PKU-HKU Joint Laboratory in Rare Earth Materials and Bioinorganic Chemistry, College of Chemistry and Molecular Engineering, Peking University, Beijing 100871, China

²State Key Laboratory of Silicon Materials, Key Laboratory of Advanced Materials and Applications for Batteries of Zhejiang Province and School of Materials Science and Engineering, Zhejiang University, Hangzhou 310027, China

[§]These authors contributed equally to this work.

Supporting information to DOI 10.1007/s12274-014-0632-7

Methods

Hydrothermal synthesis of Pt NCs. 100 mg of PVP, 63 mg of ammonium formate and 1 g of KBr were loaded into a Teflon-lined container and dissolved in 8 mL of deionized water. 0.03 mmol of K_2PtCl_4 was dissolved in the solution and the solution was diluted to 15 mL by adding deionized water. The container was then sealed in the autoclave and transferred into an oven kept at 160 °C. The autoclave was taken out after 4 h and cooled to room temperature. The black product was separated by centrifugation and washed once by $NH_3 \cdot H_2O$ (9%). The post-treatment of Pt NCs was the same that of Pt–Ni alloy NCs. The as-obtained black product was dispersed in HAc (99.9%) and treated with ultrasound for 5 h. The NCs were then collected by centrifugation and re-dispersed in ethanol. Carbon black with four times the weight of metal was then added to the ethanol dispersion and the mixture was treated with ultrasound for another 5 h. The NCs/carbon black composites were then collected by centrifugation and washed five times by deionized water. Finally, the composites were dispersed in 2 mL of ethanol for further electrochemical tests.

Synthesis of reference samples in Figure 1(b)

HCOONa. 100 mg of PVP, 2 g of KBr, 0.03 mmol of K_2PtCl_4 , 0.06 mmol of $NiCl_2$, and 68 mg of sodium formate were dissolved in 15 mL of deionized water. Hydrothermal reaction was carried out at 160 °C for 8 h. Then the black product was collected by centrifugation.

HCOONH₄. 100 mg of PVP, 2 g of KBr, 0.03 mmol of K_2PtCl_4 , 0.06 mmol of $NiCl_2$, and 63 mg of ammonium

Address correspondence to ywzhang@pku.edu.cn

formate were dissolved in 15 mL of deionized water. Hydrothermal reaction was carried out at 160 °C for 8 h. Then the black product was collected by centrifugation.

NaBH₄. 10 mg of PVP, 2 g of KBr, 0.03 mmol of K₂PtCl₄, 0.06 mmol of NiCl₂ were dissolved in 15 mL of deionized water. 0.6 mmol of NaBH₄ were then added into the solution and the solution turned black immediately. When no obvious bubbles could be seen, the black product was collected by centrifugation.

Test of the etching ability of water under hydrothermal conditions. 6 mg of Ni powder was immersed in 15 mL of an aqueous solution containing 100 mg of PVP, 63 mg of HCOONH₄, 2.5 g of KCl and 38 μL of NH₃·H₂O (25%–28%) in a 25 mL Teflon-lined container sealed in a stainless steel autoclave. The autoclave was kept at 160 °C for 8 h. After the autoclave was cooled and the excess Ni powder was removed by centrifugation, and the concentration of Ni in the solution was examined by ICP–AES.

Characterization

TGA. Thermogravimetric analyses (TGA) were conducted in N₂ flow on a Q600SDT TG-DSC analyzer (Thermal Analysis, U.S.). The rate of temperature increase was 10 °C·min⁻¹.

FT-IR. Fourier transform infrared (FT-IR) spectra of PtNi-Cl-3 and pure PVP were obtained from a VECTOR 22 FT-IR spectrometer (Bruker, Germany). To avoid the interference of carbon black on the IR spectra, un-supported Pt–Ni NCs were used for IR spectra collection. First, ~10 mg of the HAc treated PtNi-Cl-3 was dispersed to 0.5 mL using ethanol in a centrifuge tube and labeled as “acid treated”, and 2.5 μL of the dispersion was used for IR spectrum collection. This sample was then centrifuged and washed five times by deionized water, followed by re-dispersion to 0.5 mL by ethanol. 2.5 μL of this dispersion was used to take the IR spectrum as “washed by water”. The rest of the dispersion was drop-cast on a glass slide and dried, and the slide was placed under UV radiation for 5 h. The sample on the slide was then washed twice by deionized water and re-dispersed to 0.5 mL by ethanol. 2.5 μL of this dispersion was used to take the IR spectrum as “UV–ozone treated”. For every sample, 2.5 μL of the dispersion was dropped to 100 mg KBr and dried. This mixture was then ground and pressed into a disk with a diameter of 1 cm and used for IR spectrum collection.

Figures

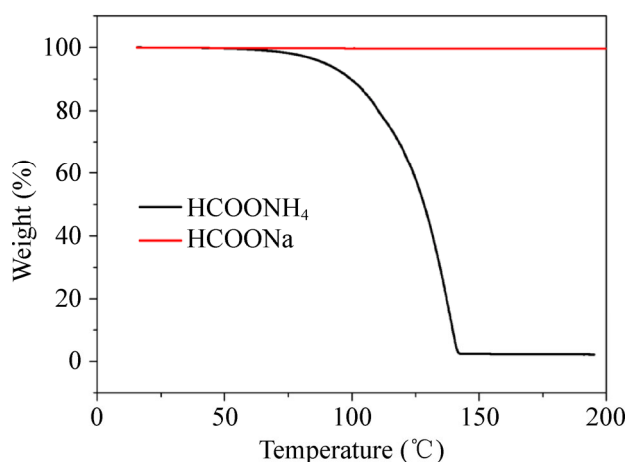


Figure S1 Thermogravimetric analyses of HCOONH₄ (black line) and HCOONa (red line) in N₂ flow.

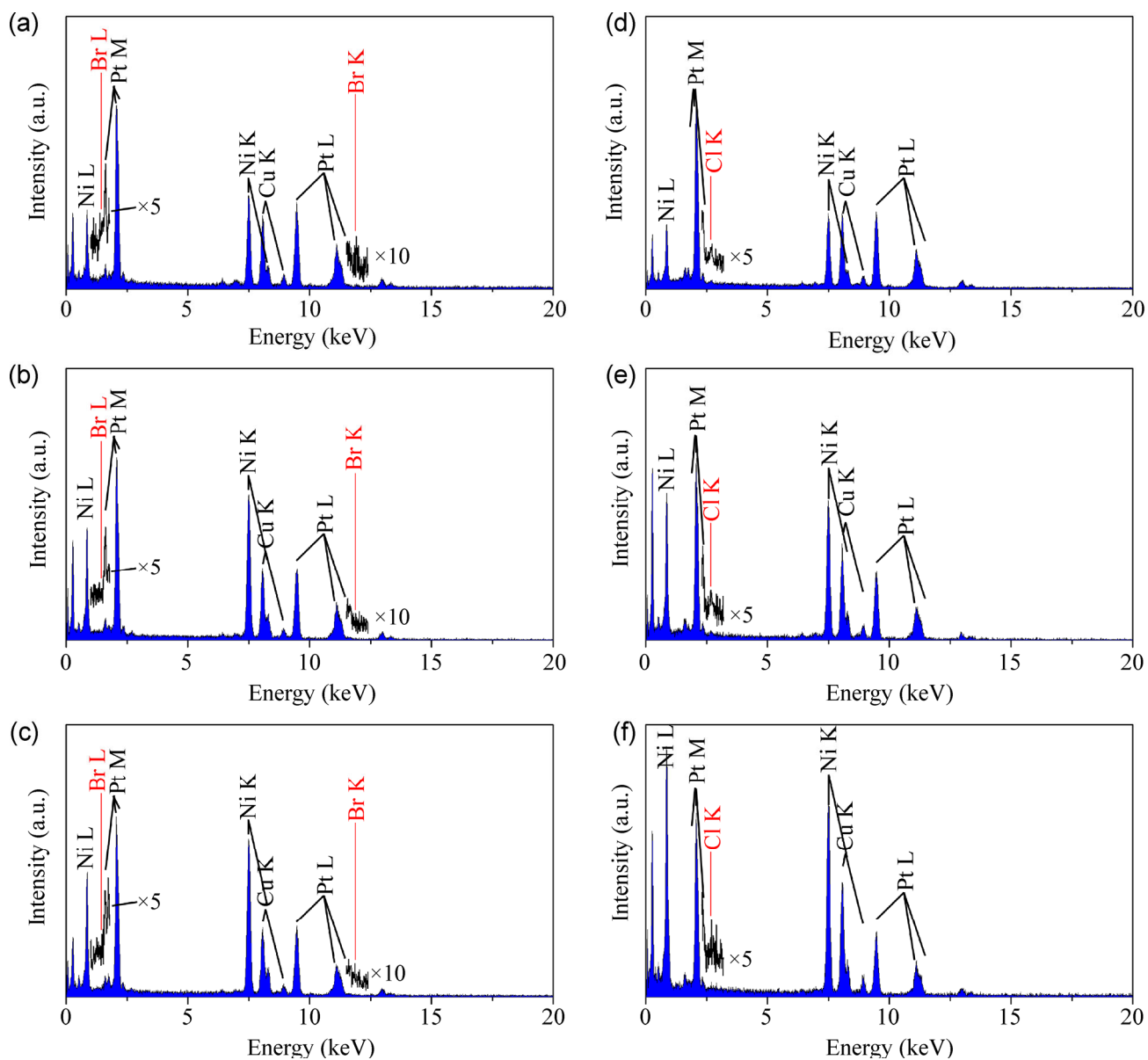


Figure S2 EDS spectra of (a) PtNi-Br-1, (b) PtNi-Br-2, (c) PtNi-Br-3, (d) PtNi-Cl-1, (e) PtNi-Cl-1 and (f) PtNi-Cl-1. K-line of Ni and L-line of Pt were used to calculate the Pt:Ni molar ratio. The regions of Br K, Br L and Cl K are magnified and the peaks originating from Br and Cl are labeled. The atomic ratio of halide ions $n(X)/(n(\text{Pt})+n(\text{Ni}))$ was lower than 0.3% for every sample.

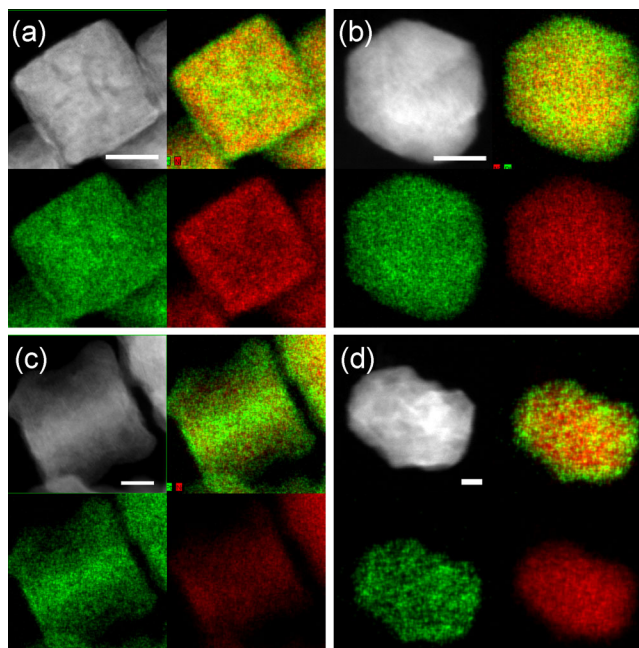


Figure S3 HAADF-STEM images (upper left), merged EDS mappings (upper right), Pt channels (lower left, green) and Ni channels (lower right, red) of (a) PtNi-Br-1, (b) PtNi-Cl-1, (c) PtNi-Br-3 and (d) PtNi-Cl-3 after HAc treatment.

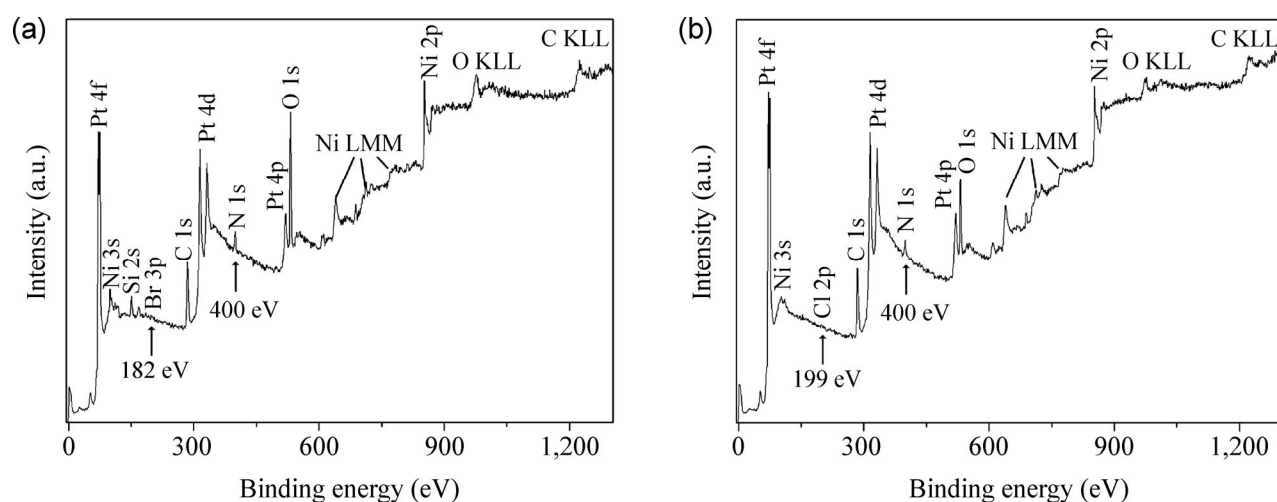


Figure S4 Survey of XPS spectra of (a) PtNi-Br-3 and (b) PtNi-Cl-3. Weak N 1s peaks at 400 eV correspond to N atoms in PVP adsorbed on the NCs. The absence of signal of Br (3p, 182 eV) and Cl (2p, 199 eV) suggests halide ions had been removed from the sample during the washing procedure.

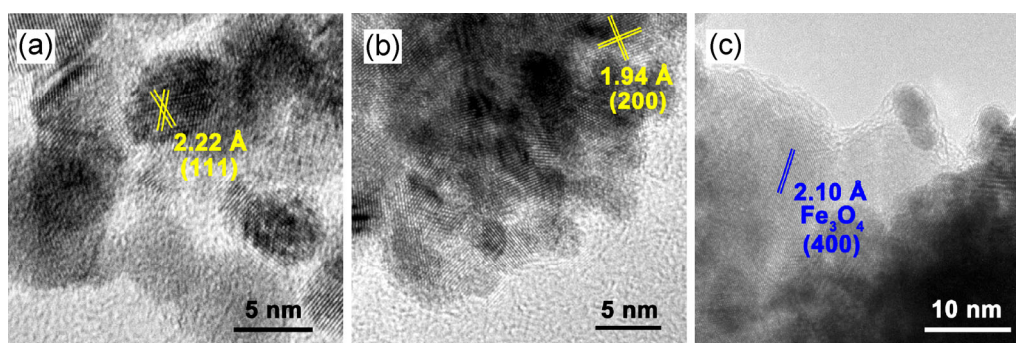


Figure S5 HRTEM images of (a) PtCo-Cl-1, (b) PtFe-Cl-1 and (c) a single Fe_3O_4 particle in PtFe-Cl-1.

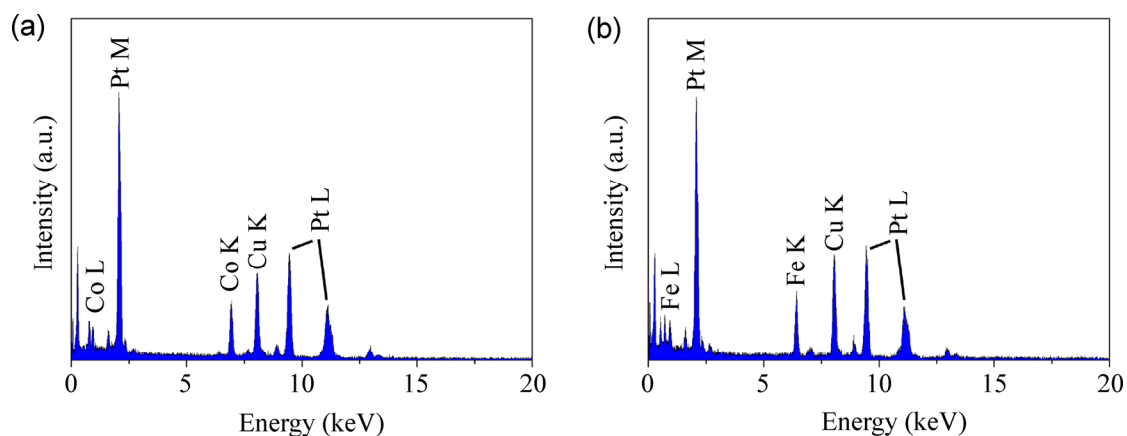


Figure S6 EDS spectra of (a) PtCo-Cl-1 and (b) PtFe-Cl-1. K-lines of Co and Fe and L-line of Pt were used for quantitative calculation.

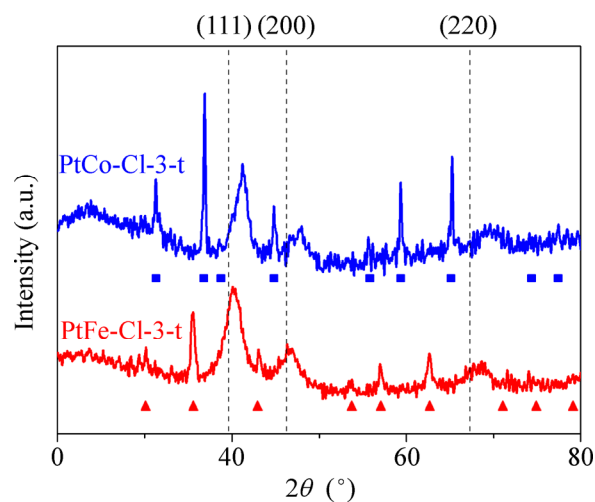


Figure S7 XRD patterns of PtCo-Cl-3 (blue line) and PtFe-Cl-3 (red line). The positions of standard diffraction peaks of pure Pt (no. 01-1190) are marked by vertical dashed lines. Blue squares and red triangles mark the label the position of standard diffraction peaks of Co_3O_4 (no. 09-0418) and Fe_3O_4 (no. 01-1111), respectively.

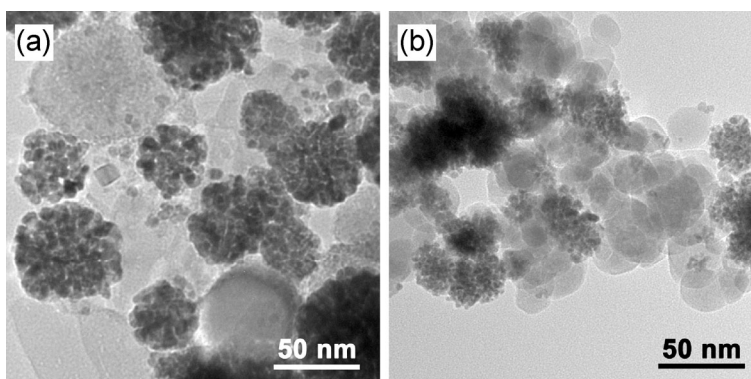


Figure S8 TEM images of (a) PtCo-Cl-3 and (b) PtFe-Cl-3.

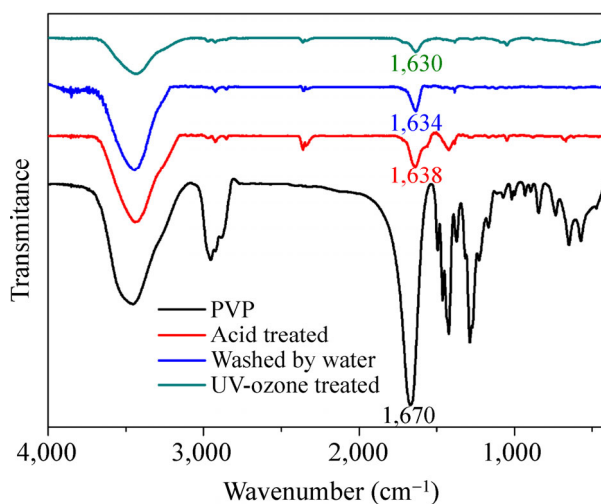


Figure S9 FT-IR spectra of Pt–Ni alloy NCs as treated by HAc (red line), washed five times by deionized water (blue line), after UV–ozone treatment (green line) and pure PVP (black line). The same amounts of the NCs were used for data collection (see Methods above). Peaks at 1,630–1,638·cm⁻¹ correspond to the stretching vibration of C=O bonds, indicating the presence of a trace of PVP. Compared with pure PVP, the peak of C=O stretching vibration shifted to lower wavenumber, suggesting PVP molecules were adsorbed on the surface of NCs through the coordination between O and surface Pt atoms [S1]. After the water-washing, UV–ozone treatment and further washing, the intensity of this peak decreased to about half of that of the as-acid-treated sample, indicating part of the adsorbed PVP molecules could be removed through these procedures.

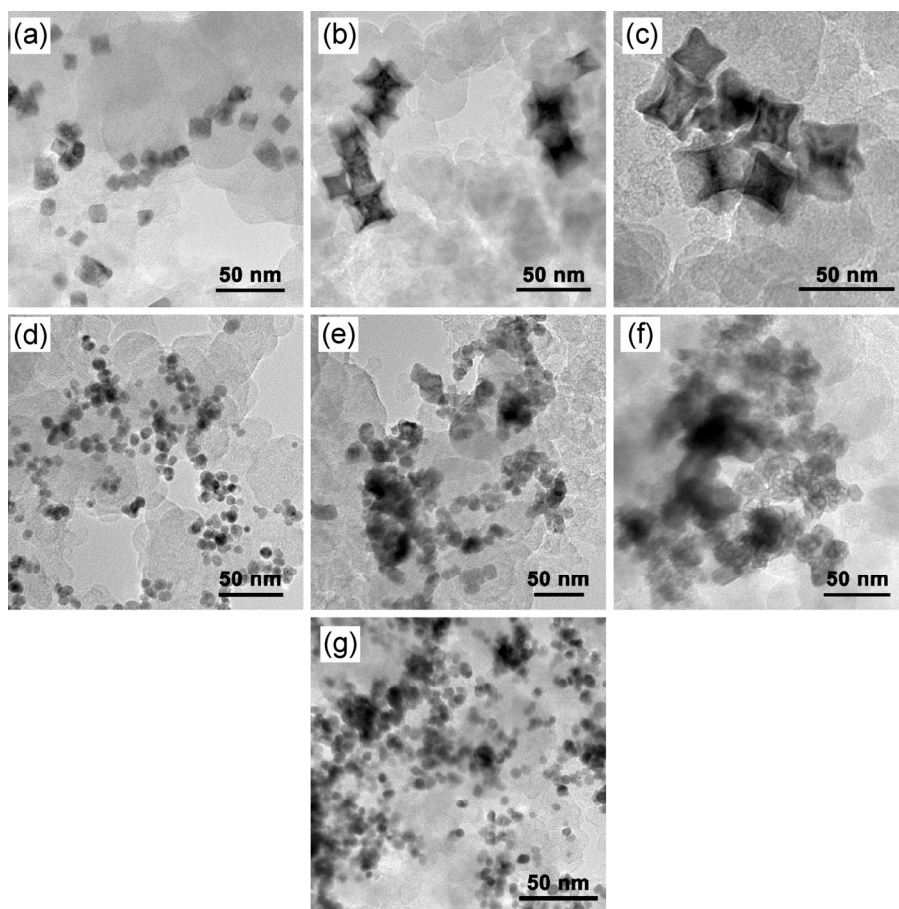


Figure S10 TEM images of (a) PtNi-Br-1, (b) PtNi-Br-2, (c) PtNi-Br-3, (d) PtNi-Cl-1, (e) PtNi-Cl-2 (f) PtNi-Cl-3 and (g) hydrothermally synthesized Pt NCs supported on carbon black Vulcan XC-72R.

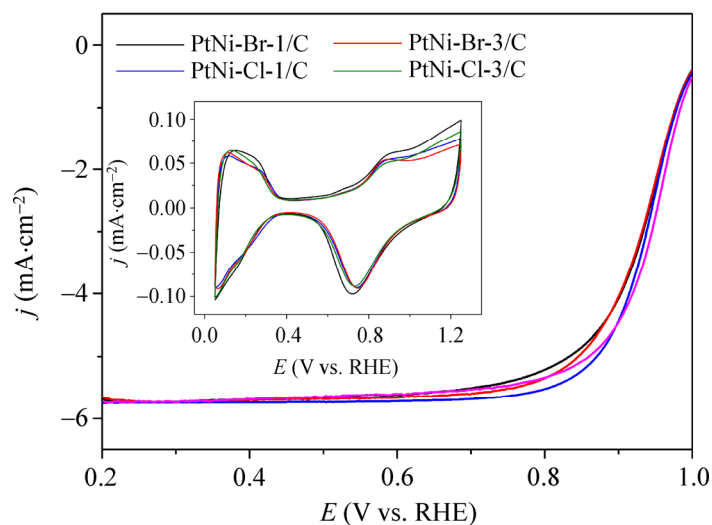


Figure S11 ORR polarization curves after iR-compensation and (inset) CV curves of PtNi-Br-1/C, PtNi-Br-3/C, PtNi-Cl-1/C and PtNi-Cl-3/C. The Pt loading amount of each sample was $5.0 \mu\text{g}$. CV curves were collected with a scan speed of $50 \text{ mV}\cdot\text{s}^{-1}$ in N_2 saturated 0.1 M HClO_4 . The current density was normalized to the ECSA. ORR polarization curves were collected on a rotating disk electrode (RDE) with a rotation speed of $1,600 \text{ rpm}$ in the anodic scan with a scan speed of $20 \text{ mV}\cdot\text{s}^{-1}$ in O_2 saturated 0.1 M HClO_4 . The current density was normalized to the geometric area of RDE.

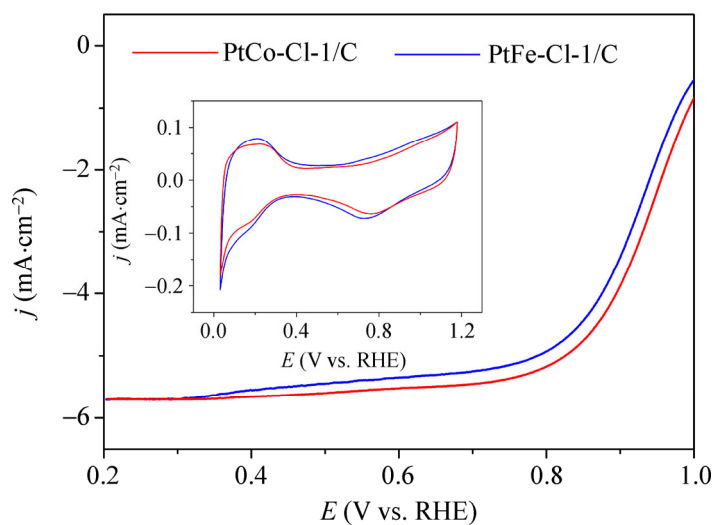


Figure S12 ORR polarization curves after iR-compensation and (inset) CV curves of PtCo-Cl-1/C and PtFe-Cl-1/C. The Pt loading amount of each sample was $5.0 \mu\text{g}$. CV curves were collected with a scan speed of $50 \text{ mV}\cdot\text{s}^{-1}$ in N_2 saturated 0.1 M HClO_4 . The current density was normalized to the ECSA. ORR polarization curves were collected on a rotating disk electrode (RDE) with a rotation speed of $1,600 \text{ rpm}$ in the anodic scan with a scan speed of $20 \text{ mV}\cdot\text{s}^{-1}$ in O_2 saturated 0.1 M HClO_4 . The current density was normalized to the geometric area of RDE.

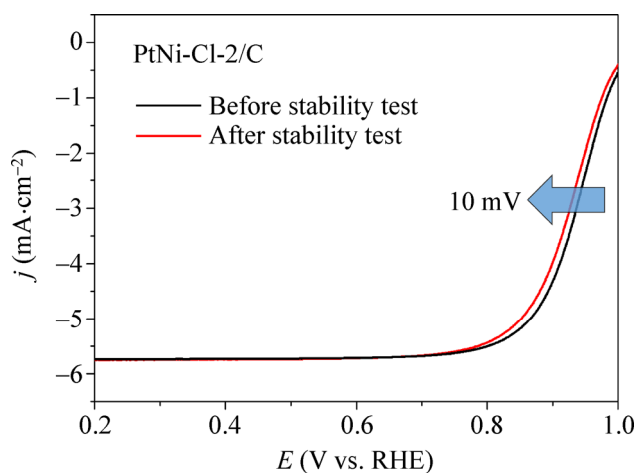


Figure S13 ORR polarization curves of PtNi-Cl-2/C before (black) and after (red) 10,000 cycles of voltage sweeps between 0.6 and 1.0 V in N_2 saturated 0.1 M $HClO_4$ solution with the scan rate of $50\text{ mV}\cdot\text{s}^{-1}$.

Tables

Table S1 Rietveld analysis of Pt–Ni alloy nanocrystals

| Sample ID | Lattice parameter (Å) | Pt molar fraction | Ni molar fraction | Phase (wt.%) | Average crystallite size (nm) | Total Pt:Ni molar ratio |
|-----------|-----------------------|-------------------|-------------------|--------------|-------------------------------|-------------------------|
| PtNi-Br-1 | 3.77(7) | 0.61 | 0.39 | 100 | 7.6 | 61:39 |
| PtNi-Br-2 | 3.73(6) | 0.51 | 0.49 | 92 | 5.9 | 49:51 |
| | 3.66(3) | 0.32 | 0.68 | 8 | 16.7 | |
| PtNi-Br-3 | 3.72(2) | 0.47 | 0.53 | 71 | 3.3 | 38:62 |
| | 3.618(8) | 0.21 | 0.79 | 29 | 16.7 | |
| PtNi-Cl-1 | 3.75(0) | 0.54 | 0.46 | 100 | 5.6 | 54:46 |
| PtNi-Cl-2 | 3.77(2) | 0.60 | 0.40 | 45 | 3.2 | 38:62 |
| | 3.637(6) | 0.26 | 0.74 | 55 | 5.8 | |
| PtNi-Cl-3 | 3.73(1) | 0.50 | 0.50 | 41 | 2.9 | 29:71 |
| | 3.607(8) | 0.19 | 0.81 | 59 | 9.1 | |

Table S2 XPS data fitting in the Pt 4f region of unsupported hydrothermally synthesized Pt–Ni alloy NCs and Pt NCs after HAC treatment

| Sample ID | Pt^0 | | Pt^{2+} | | Pt^{4+} | |
|-----------|------------------------|----------------|-----------|----------------|-----------|----------------|
| | B.E. (eV) ^a | Percentage (%) | B.E. (eV) | Percentage (%) | B.E. (eV) | Percentage (%) |
| PtNi-Br-1 | 71.2 | 47 | 71.8 | 30 | 73.4 | 23 |
| PtNi-Br-2 | 71.3 | 52 | 71.9 | 29 | 74.1 | 19 |
| PtNi-Br-3 | 71.2 | 50 | 71.8 | 31 | 73.7 | 19 |
| PtNi-Cl-1 | 71.3 | 49 | 71.8 | 31 | 73.3 | 20 |
| PtNi-Cl-2 | 71.1 | 54 | 71.7 | 27 | 73.9 | 19 |
| PtNi-Cl-3 | 71.2 | 47 | 71.8 | 33 | 73.8 | 20 |
| Pt NCs | 71.2 | 40 | 71.8 | 38 | 73.7 | 22 |

^a The binding energy of Pt $4f_{7/2}$ peaks.

Table S3 Sample identification, reagents and composition analysis of hydrothermally synthesized Pt-*M* (*M* = Co, Fe) alloy NCs

| Sample ID | K ₂ PtCl ₄ (mmol) | <i>M</i> precursor | Amount (mmol) | Pt: <i>M</i> feeding ratio | Additive | Pt: <i>M</i> molar ratio | | |
|-----------|--|--------------------|------------------|-------------------------------|------------|--------------------------|----------------|------------------|
| | | | | | | ICP | EDS | XRD ^a |
| PtCo-Cl-1 | 0.06 | CoCl ₂ | 0.06 | 1:1 | KCl, 2.5 g | 70:30 | 71:29 | 74:26 |
| PtCo-Cl-3 | 0.04 | CoCl ₂ | 0.12 | 1:3 | KCl, 2.5 g | – ^b | – ^b | 64:36 |
| PtFe-Cl-1 | 0.06 | FeSO ₄ | 0.06 | 1:1 | KCl, 2.5 g | 68:32 | 73:27 | 87:13 |
| PtFe-Cl-3 | 0.04 | FeSO ₄ | 0.12 | 1:3 | KCl, 2.5 g | – ^b | – ^b | 80:20 |

^a The Pt:*M* molar ratios were calculated according to Vegard's law from (111) diffraction peaks. The JCPDS card numbers for pure fcc Co and fcc Fe (calculated) were 15-0806 and 52-0513, respectively.

^b Due to the presence of large amounts of Co₃O₄ or Fe₃O₄, the Pt:*M* molar ratio in the alloy could not be obtained from ICP–AES and EDS.

Table S4 ECSA, ORR specific activity and resistance of different samples

| Sample ID | ECSA _H (m ² ·g _{Pt} ^{−1}) ^a | ECSA _{CO} (m ² ·g _{Pt} ^{−1}) ^b | ECSA _{CO} / ECSA _H | <i>j</i> _H (mA·cm ^{−2}) ^c | <i>j</i> _{CO} (mA·cm ^{−2}) ^d | <i>R</i> (Ω) |
|----------------------|--|---|---|--|---|--------------|
| PtNi-Br-1/C | 40 ± 3 | 41 ± 3 | 1.03 ± 0.01 | 1.48 ± 0.11 | 1.44 ± 0.12 | 16.3 ± 0.1 |
| PtNi-Br-2/C | 37 ± 3 | 38 ± 4 | 1.04 ± 0.03 | 2.25 ± 0.10 | 2.17 ± 0.15 | 20.3 ± 0.3 |
| PtNi-Br-3/C | 33 ± 4 | 32 ± 3 | 0.98 ± 0.03 | 1.76 ± 0.14 | 1.79 ± 0.09 | 17.2 ± 0.3 |
| PtNi-Cl-1/C | 47 ± 2 | 49 ± 3 | 1.05 ± 0.01 | 1.76 ± 0.13 | 1.68 ± 0.14 | 17.5 ± 0.2 |
| PtNi-Cl-2/C | 37 ± 5 | 38 ± 5 | 1.05 ± 0.03 | 2.69 ± 0.12 | 2.62 ± 0.12 | 16.4 ± 0.4 |
| PtNi-Cl-3/C | 51 ± 4 | 51 ± 4 | 1.00 ± 0.02 | 1.67 ± 0.04 | 1.66 ± 0.04 | 19.8 ± 0.7 |
| PtCo-Cl-1/C | 50 ± 6 | 49 ± 5 | 0.99 ± 0.04 | 1.02 ± 0.11 | 1.03 ± 0.10 | 21.0 ± 0.7 |
| PtFe-Cl-1/C | 65 ± 4 | 63 ± 4 | 0.97 ± 0.02 | 0.53 ± 0.07 | 0.54 ± 0.06 | 19.3 ± 0.9 |
| Commercial Pt/C | 84 ± 5 | 81 ± 4 | 0.96 ± 0.02 | 0.20 ± 0.02 | 0.21 ± 0.02 | 15.2 ± 0.1 |
| Hydrothermal Pt/C | 42 ± 7 | 41 ± 7 | 0.98 ± 0.02 | 0.21 ± 0.04 | 0.21 ± 0.03 | 17.2 ± 0.4 |

^a ECSA calculated from H UPD charge.

^b ECSA calculated from CO stripping charge.

^c ORR specific activity normalized to ECSA_H.

^d ORR specific activity normalized to ECSA_{CO}.

References

- [S1] Wang, H. S.; Qiao, X. L.; Chen, J. G.; Wang, X. J.; Ding, S. Y. Mechanisms of PVP in the preparation of silver nanoparticles. *Mater. Chem. Phys.* **2005**, *94*, 449–453.